IEEE Access
Multidisciplinary | Rapid Review | Open Access Journal

Received July 21, 2019, accepted August 5, 2019, date of publication August 12, 2019, date of current version August 23, 2019.

Digital Object Identifier 10.1109/ACCESS.2019.2934652

Traveling-Wave Series-Fed Patch Array Antenna Using Novel Reflection-Canceling Elements for Flexible Beam

HAO YI, LONG LI, (Senior Member, IEEE), JIAQI HAN, AND YAN SHI, (Senior Member, IEEE)
Key Laboratory of High-Speed Circuit Design and EMC of Ministry of Education, School of Electronic Engineering, Xidian University, Xi'an 710071, China

Corresponding author: Long Li (lilong@mail.xidian.edu.cn)

This work was supported in part by the Shaanxi Outstanding Youth Science Foundation under Grant 2019JC-15, and in part by the National Key Research and Development Program of China.

ABSTRACT The methodology of designing traveling-wave series-fed patch array antennas (TSPAAs) based on reflection-canceling elements for flexible radiation pattern has been proposed. By introducing a quarter-wave transformer as the reflection-canceling structure, the cascaded patch antenna with tapered width can be used as the reflection-canceling element for a nonuniformly spaced TSPAA. Because of its simple structure, the parameters of the transformer can be determined directly by the corresponding equivalent circuit. To achieve a flexible radiation pattern, the array aperture distribution can be controlled by changing the element width (for amplitude distribution) and the element spacing (for phase distribution). In this method, the initial array is synthesized through a genetic algorithm approach, and a simulation-based iterative process considering the accurate mutual coupling is developed to optimize the initial array. To evaluate the proposed method, two different types of 14-element linear arrays operating at ISM 24GHz are implemented for a low sidelobe pattern and shaped-beam pattern, respectively. The two arrays are both simulated, fabricated and measured, the measured results show reasonable agreement with the simulation results, which verifies the effectiveness and correctness of the proposed method in this paper.

INDEX TERMS Genetic algorithm (GA), low sidelobe pattern, reflection-canceling element, simulation-based iteration procedure, shaped-beam pattern, traveling-wave series-fed patch array antenna (TSPAA).

I. INTRODUCTION

The microstrip patch array antenna is widely used in wireless communication systems and microwave radar sensors for its attractive properties, such as light weight, low profile, low cost and easy integration [1], [2]. Moreover, the desired radiation patterns with high gain, low sidelobe or shaped beam can be obtained flexibly [3]–[6]. Depending on the feeding scheme [7], microstrip patch arrays could be divided into categories, the parallel-fed array and the series-fed array. In spite of the naturally narrow-band characteristic, the series-fed patch array has more brief and compact feed scheme and hence higher antenna efficiency and lower spurious radiation than the parallel-fed patch array, especially at millimeter wave frequency [8]. Plenty of standing-wave series-fed patch array antennas have been developed with low sidelobe pattern, whose elements are excited with various tapered amplitude distributions, such as Dolph-Chebyshev distribution or Taylor distribution [9]–[12]. However, the standing-wave series-fed patch array cannot obtain the shaped beam pattern or other asymmetric patterns due to the in-phase excitation, which limits its application. Different from the standing-wave array, the phase excitation and amplitude excitation in a traveling-wave series-fed patch array antenna (TSPAA) can be adjusted simultaneously, thus providing the possibility to obtain an arbitrary radiation pattern. Therefore, the method of designing TSPAAs with various patterns have received considerable attention [13]–[18].

Traditional TSPAAs generally offset the element spacing from the resonant length to obtain impedance matching. In this way, the reflected waves from elements cancel each other to obtain traveling wave on the main feeding line [13]–[16]. However, it brings about some defects. First, the non-in-phase excitation causes the main beam of the array pattern to deviate from broadside. Second, the matching load deteriorates the array antenna efficiency. Third, the radiation

The associate editor coordinating the review of this article and approving it for publication was Guan-Long Huang.

power of each array element has to be much less than the input power. Otherwise, the cumulative reflection will lead to a dramatic error between the actual aperture distribution and the ideal aperture distribution, especially for the low-sidelobe array and shaped-beam array which require more accurate aperture distributions.

Several synthesis methods based on the circuit model have been reported for the non-uniformly spaced TSPAAs [17], [18]. In [17], a circuit representation of the patches in the array environment was given, with the parameters of the patches determined experimentally. However, the array antenna efficiency is relatively low due to the absorbing load. Besides, the broadside radiation pattern cannot be obtained by this method. In [18], the circuit model of the series-fed array was equivalent to non-uniformly spaced slots connected by high-impedance and low-impedance transmission line. However, the method ignores the mutual coupling between the elements, leading to an increase in the error of the array aperture distribution, especially for millimeter-wave frequency bands. Besides the series-fed patch array, other simple printed structures without a feeding network are proposed to achieve high-directivity patterns [19].

To solve the problems mentioned above, a promising method based on the reflection-canceling element is proposed [20]–[27]. With introduced reflection-canceling structures, the reflections caused by the array elements can be suppressed to achieve approximate traveling wave on the feeding line. Consequently, the in-phase excitations and large coupling power are allowed for the TSPAAs. The reflection-canceling element is first proposed for designing waveguide slot array antenna [20]–[24]. By introducing a matching slot pair [20], an inductive vertical post [21], and an associated wall [22] near the waveguide slot antenna, the reflection from the slot element can be canceled due to the alternating-phase reflection from these introduced structures. In [22], a center feed single layer slotted waveguide array with the reflection-canceling slot element was presented to suppress cumulative reflection and assure the boresight beam. Then, the method is extended to design the SIW slot antenna array [23], where the inductive post in [21] was replaced by the plated via. With the similar reflection-canceling element, an 8-element SIW slot array with broadside radiation pattern is designed with -22.5dB sidelobe level (SLL) [24].

Due to the fact that the series-fed patch array has the similar working principles to the waveguide slot array, the reflection-canceling element is adopted to design traveling-wave patch arrays. The millimeter-wave microstrip comb-line antennas with reflection-canceling structures were presented [25]–[27]. In [25], a reflection-canceling slit structure was installed on the feeding line around each radiating element, and therefore a broadside radiation pattern with -17.9dB SLL was achieved through a 27-element linear array. To enhance the coupling power of element, the matching stub was introduced in parallel to the wider radiating element, and therefore the SLL was reduced to -30dB in a 14-element and a 6-element array [26]. In [27], the stub-studded radiating element was employed to broaden the impedance bandwidth. However, the above slit structures on the feeding lines may lead to increase cross polarization and manufacturing problems at millimeter-wave frequencies. Besides, other radiation patterns such as a shaped beam have not been mentioned in these designs. Consequently, a novel reflection-canceling element with simple structure is desired for TSPAAs to synthesize flexible radiation patterns.

In this work, the method of designing a TSPAA with novel reflection-canceling patch elements is proposed. First, the novel reflection-canceling element composed of a cascaded rectangle patch and an additional quarter-wave impedance transformer is devised. The impedance transformer acts as the reflection-canceling structure for reducing the reflection. According to the equivalent circuit model of the proposed element, the parameters of the impedance transformer can be calculated directly. Then, the configuration of a typical TSPAA consisting of multiple reflection-canceling elements and a radiating matched element (RML) is studied. Thanks to the use of the reflection-canceling elements, an arbitrary radiation pattern can be achieved through independent control of the amplitude and phase aperture distribution, which can be realized by changing element width and element spacing, respectively. Based on this, the initial array is synthesized through a genetic algorithm (GA) approach. After that, a simulation-based iterative process with taking into account the accurate mutual coupling between different array elements is proposed to optimize the initial array. As a result, the error of the actual aperture distribution can be reduced. To evaluate the proposed method, two types of linear arrays with low sidelobe and shaped beam are respectively designed, simulated and tested. Measured results confirm the effectiveness and correctness of the proposed method.

II. DESIGN OF ANTENNA ELEMENTS

A. REFLECTION-CANCELING ELEMENT

The geometry of the proposed novel reflection-canceling element is shown in Fig. 1(a), which is composed of a rectangular patch, a microstrip feeding line through the patch and a quarter-wave impedance transformer attached directly to the patch. The key point is that the quarter-wave impedance transformer is introduced as the reflection-canceling structure to suppress the reflection. Thus, the traveling wave can be realized on the feeding line, in which a part of the input power from the port 1 will be radiated by the patch antenna and the rest is delivered to the port 2 acting as the input port for the next cascade.

The equivalent circuit representation for the rectangular patch antenna is given in [1]. Assuming that the radiating patch is in resonance, the equivalent circuit of the proposed element can be depicted in Fig. 1(b). The resonant radiating conductance of the patch and the characteristic admittance of the impedance transformer are represented by G^{trans} and G^{pat}, respectively. Both their values are normalized to G_0, the characteristic admittance of the feeding line. It is expected

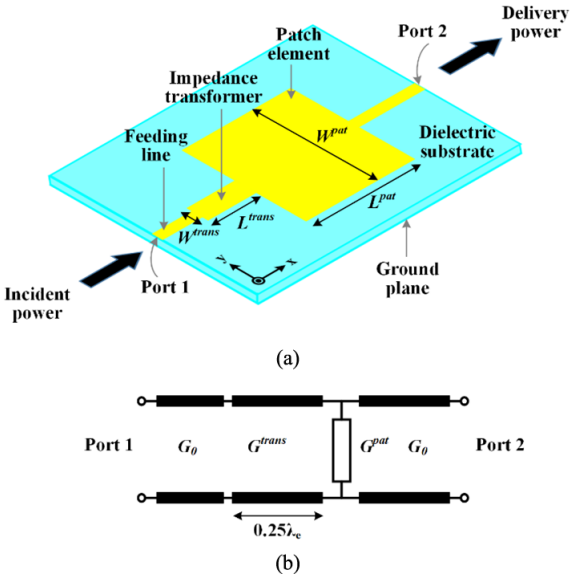

FIGURE 1. Geometry and equivalent circuit model of proposed reflection-cancelling patch element. (a) Geometry and (b) equivalent circuit model.

that the next cascade should be kept to match, hence the input impedance of port 2 can be replaced by a matching load. In order to suppress the reflection from the patch element, in other words to maintain traveling wave along the feeding line, the proposed antenna element has to be well matched to the characteristic impedance of the feeding line. Thus, the characteristic admittance of the impedance transformer G^{trans} can be calculated by

$$G^{trans} = sqrt(1 + G^{pat}) \tag{1}$$

For the reason that the impedance transformer has less impact on the resonance of the rectangular patch, the parameters of the impedance transformer can be directly determined when the radiating conductance of the patch is given. As a comparison, the parameters of the reflection-canceling structure in [25]–[27] have to be tuned carefully to obtain impedance matching. In addition, the characteristic conductance of the impedance transformer G^{trans} is larger than 1 from (1), hence the width of the impedance transformer is always larger than the feeding line width. As a result, the proposed reflection-canceling element in this paper are more robust to manufacturing tolerances than that in [25]–[27].

B. PARAMETERS EXTRACT

In order to design a TSPAA, the parameter curves of the proposed reflection-canceling element, including the patch radiation conductance G^{pat}, the patch length L^{pat}, the feeding line length L^{fl}, the transformer length L^{trans} and the transformer width W^{trans}, over the patch width W^{pat} have to be extracted. Due to the open-end effect [1], the resonant lengths of the patch and the feeding line are slightly less than the half wavelength. In addition, the mutual coupling between the cascaded patches has to be considered. In this work, the full-wave simulation experiments in a uniform

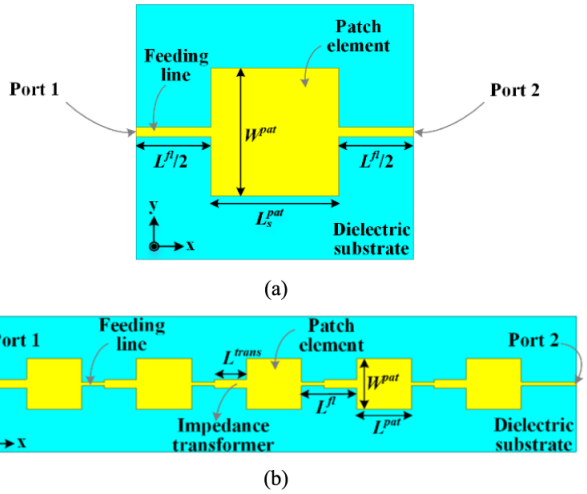

FIGURE 2. Full-wave simulation model to extract resonant parameters. (a) Single patch and (b) uniform patch array.

array environment are conducted to obtain the parameter curves. The high frequency simulation software (HFSS 15) is employed. In a simulation experiment, the following steps are taken to extract the resonant parameters while keeping patch width unchanged W^{pat}.

STEP 1: A single patch model shown in Fig. 2(a) is used to extract the initial resonant parameters of the patch without taking into account the mutual coupling. Tuning the length of the patch and de-embedding the length of the feeding line to make

$$\text{Im}\,(S_{11}) = 0, \tag{2}$$
$$\text{ang}\,(S_{12}) = 0. \tag{3}$$

Thus, the resonant length of the feeding line L_s^{fl}, and the resonant length of patch L_s^{pat} under taking the open-end effect into account can be obtained. The radiating conductance of the resonant patch antenna G_s^{pat} can be obtained from

$$G_s^{pat} = \frac{1 - S_{11} - S_{12}}{S_{12}}. \tag{4}$$

STEP 2: The characteristic admittance G^{trans} of the impedance transformer can be derived from (1). Thus, the transformer length L^{trans} and transformer width W^{trans} can be easily acquired by HFSS simulation.

STEP 3: A uniform array consists of 5 constant-width elements shown in Fig. 2(b) is applied to extract the patch length and the radiating conductor with taking into account the mutual coupling. The similar process can be found in [17], where the experiments are conducted instead. The element spacing is set as L_s^{fl} from Step 1, and the initial parameters of the patch and the impedance transformer are obtained from Step 1 and Step 2, respectively. By fine tuning the length of the patch L^{pat} and the length of the feeding line L^{fl}, we can make

$$\text{Im}\,(S_{11}) = 0 \tag{5}$$
$$\theta_m = 0 \tag{6}$$

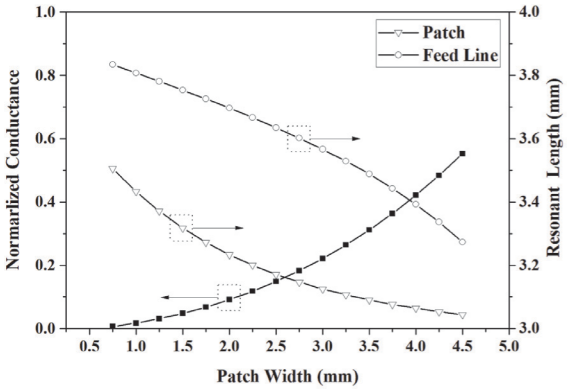

FIGURE 3. Normalized conductance curve, resonant patch length curve and resonant feed line length curve over patch width at 24.125GHz.

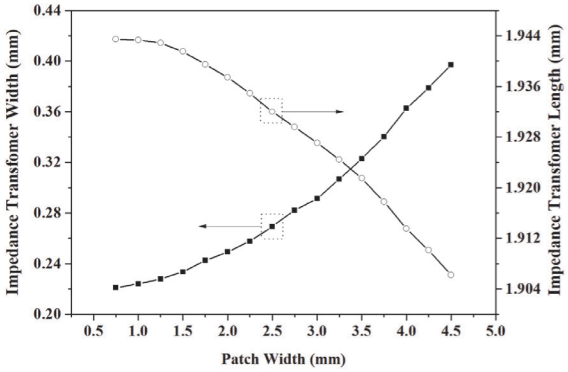

FIGURE 4. Length curve and width curve of quarter-wave impedance transformer over patch width at 24.125GHz.

where θ_m is the angle between the Z axis and the direction of maximum radiation. Thus, the resonant length of the feeding line L^{fl} and the resonant length of the patch L^{pat} can be obtained. The radiating conductance of the patch G^{pat} can be obtained from

$$G^{pat} = (S_{12})^{-0.2} - 1 \tag{7}$$

In this work, the antenna operates at 24GHz ISM band, covering from 24GHz to 24.25GHz. The proposed antenna is printed on a dielectric substrate Rogers RO4350B (relative dielectric constant $\varepsilon_r = 3.66$ and loss tangent $\tan\delta = 0.004$) with a thickness of 0.508mm. The feed line with characteristic impedance of 100 Ω, whose width is 0.22mm, is applied to avoid the feeding line too wide and the radiating admittance too small. The variation range of the patch width is limited from 0.75mm to 4.5mm. Repeating this simulation experiment, the parameter curves over the patch width can be obtained. The resonant patch length L^{pat}, the resonant feeding line length L^{trans} and the resonant patch conductance G^{pat} depending on the patch width W^{pat} are shown in Fig. 3. The transformer width W^{trans} and the transformer length L^{trans} varying with the patch width W^{pat} are shown in Fig. 4.

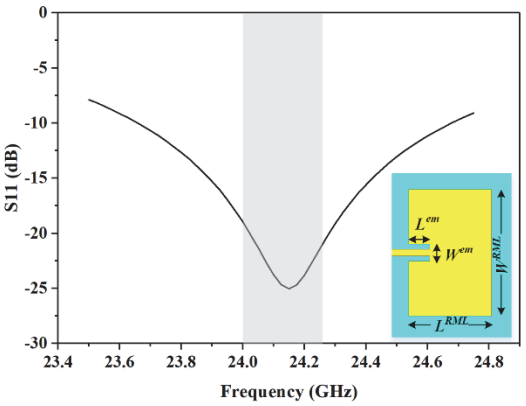

FIGURE 5. Structure and reflection coefficient of the RML ($W^{RML} = 4.5$mm, $W^{EM} = 0.6$mm, $L^{EM} = 0.75$ mm).

C. RADIATING MATCHED LOAD

The traditional TSPAAs suffer the low radiation efficiency due to the large dissipation from dielectric loss, conduct loss, and leakage loss. In the 24GHz ISM band, the efficiency problem will be more critical. Thus, a radiating matching load (RML) is employed as the last element in a TSPAA to increase the radiation efficiency [24]–[26].

Fig. 5 shows the geometry of the RML. The patch element is end fed by an inserted feeding line. Through optimizations using HFSS, the RML is matched to 100Ω at the center frequency. The parameter values and the reflection coefficient of the RML are also depicted in Fig. 5. It can be seen that the impedance bandwidth of the RML can cover the whole 24GHz ISM band (24-24.25GHz).

III. ARRAY DESIGN

A. TRAVELING-WAVE ARRAY CONFIGURATION

The configuration of a typical n-elements TSPAA is shown in Fig. 6. It consists of n-1 reflection-canceling elements and the RML at the end. The radiating elements are sequentially connected by the feeding line. The width and length of the ith patch are W_i^{pat} and L_i^{pat}, and the width and length of corresponding impedance transformer are W_i^{trans} and L_i^{trans} ($i = 1, 2, \ldots, n$-1). The spacing between the ith element and the (i+1)th element is S_i^{pat} ($i = 1, 2, \ldots, n$-1). The input power is delivered by the feeding line and then radiated by the cascaded elements. In terms of the reflection-cancelling elements, traveling waves are maintained through the feeding line regardless of the exciting amplitude and phase. Consequently, there is a strong possibility that a flexible radiation pattern can be obtained by the proposed TSPAA.

According to the equivalent circuit network depicted in Fig. 6, the amplitude distribution of the linear array can be controlled by the patch width W_i^{pat}, and the phase distribution can be controlled by the element spacing S_i^{pat} offset from the resonance. However, some actual factors about the array structure must be considered. First, the variation of the patch width is limited to [0.75mm, 4.5mm]. The maximum width

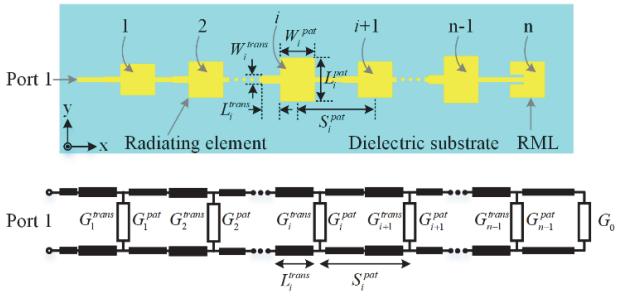

FIGURE 6. Configuration and equivalent circuit model of proposed traveling-wave array.

of the patch element is about 0.37 free space wavelengths at center frequency, which ensures reasonable space between elements when multiple linear arrays form a planar array. Second, the variation of the element spacing S_i^{pat} is limited to [5mm, 8.5mm] to avoid structure interference between the impedance transformer and the prior patch element. It is worth noting that the spacing between the RML and the (n-1)th element can be extended to [4mm, 8.5mm] because no impedance transformer is connected to the RML. Therefore, the desired array distribution for an arbitrary radiation pattern may be obtained by searching $[W_i^{pat}, S_i^{sat}]$ in above constraint conditions.

B. PATTERN SYNTHESIS USING THE GENETIC ALGORITHM

As a classic global optimization algorithm, the genetic algorithm has been widely used for synthesis of array radiation pattern for several decades [28]–[30]. In this work, the GA is applied to produce the parameters of the initial array for the desired radiation pattern. The chromosome is directly represented with $[W_i^{pat}, S_i^{sat}]$, where the RML is excluded. Thus, the dimension of the chromosome is 2(n-1).

Given patch width $[W_i^{pat}]$, the conductance $[G_i^{pat}]$ can be found from Fig. 2. It can be seen that the variation range of the radiating conductor is about [0.007,0.553]. The amplitude distribution $[A_i]$ can be determined from the equivalent circuit of the TSPAA shown in Fig. 6, which can be expressed as

$$A_i = \begin{cases} sqrt\left(\dfrac{G_i^{pat}}{1+G_i^{pat}}\right), & i=1 \\ sqrt\left(\dfrac{G_i^{pat}}{1+G_i^{pat}} * \left(1-\sum_{j=1}^{i-1} A_j^2\right)\right), & i=2,3,\ldots,n-1 \\ sqrt\left(1-\sum_{j=1}^{i-1} A_j^2\right), & i=n. \end{cases} \tag{8}$$

The phase difference $[P_i]$ between adjacent elements is realized by offset the element spacing from the resonance. Consequently, it can be written as

$$P_i = \begin{cases} -\dfrac{2\pi}{\lambda_g} * \left(S_i^{pat} - 0.5 * \left(L_i^{pat} + L_{i+1}^{pat} + L_i^{fl} + L_{i+1}^{fl}\right)\right), \\ \qquad i = 1, 2, \ldots, n-2 \\ -\dfrac{2\pi}{\lambda_g} * \left(S_i^{pat} - 0.5 * \left(L_i^{pat} + L^{RML} + L_i^{fl} + L_n^{fl}\right) - L^{em}\right), \\ \qquad i = n-1 \end{cases} \tag{9}$$

where λ_g is the wavelength of the feeding line at center frequency, L_i^{fl} is the resonant length of the feeding line for the ith reflection-canceling element and L_n^{fl} is the resonant length of the feeding line for the RML, which is 3.722 mm by electromagnetic simulations. From (9), the variation range of the phase difference is [-101.1°, 131.5°]. The phase distribution $[\Phi_i]$ is given by

$$\Phi_i = \begin{cases} 0, & i=1 \\ \sum_{j=1}^{i-1} P_j, & i=2,3,\ldots,n \end{cases} \tag{10}$$

The aperture amplitude and phase distribution of the TSPAA can be obtained from (8)-(10). Therefore, the radiation pattern of the TSPAA in the E-plane can be determined by

$$f(\theta) = \frac{\sum_{i=1}^{n} A_i * \exp\left(-j\frac{2\pi}{\lambda_0} D_i \sin\theta + \Phi_i\right) * f_i^e(\theta)}{\sum_{i=1}^{n} A_i * \exp\left(-j\frac{2\pi}{\lambda_0} D_i \sin\theta_m + \Phi_i\right) * f_i^e(\theta_m)} \tag{11}$$

$$D_i = \begin{cases} 0, & i=1 \\ \sum_{j=1}^{i-1} S_j^{pat}, & i=2,3,\ldots,n \end{cases} \tag{12}$$

$$f_i^e(\theta) = \cos\left(\frac{\pi}{\lambda_0} L_i^{pat} \sin\theta\right) \tag{13}$$

where λ_0 is the free space wavelength at center frequency, θ is the beam title angle from $+Z$ axis inclined to $+X$ directions as defined in Fig. 6, θ_m is the direction of maximum radiation, D_i is the spacing between the ith element and the first element, and $f_i^e(\theta)$ is the approximated radiation pattern of the ith element in the E-plane [31].

The fitness function, i.e., cost measure to be miniaturized, defined for this optimization is

$$\varepsilon_{cost} = w_1 * \sum_{\substack{\theta \in mainlobe, and \\ |f(\theta) - f(\theta)^i| > ripple}} \left|f(\theta) - f(\theta)^i\right|^2 + w_2 * \sum_{\substack{\theta \in sidelobe, and \\ f(\theta) > sll}} \left|f(\theta) - f(\theta)^i\right|^2 \tag{14}$$

where ε_{cost} is the cost function, $f(\theta)^i$ is the desired arbitrary radiation pattern, θ is angle range of [-90°, 90°], *ripple* is the maximum ripple allowed for the mainlobe, *sll* is the SLL allowed for the sidelobe, ω_1 is the weight of the fitness function of the mainlobe, and ω_2 is for the sidelobe. In this work, *sll* is 3dB, ω_1 is 0.7 and ω_2 is 0.3.

The code of standard GA is developed in MATLAB. Given the desired radiation pattern and the proper element number, the best chromosome $[W_i^{pat}, S_i^{pat}]$ for the initial array may be obtained through the GA process. After that, the length of the patches $[L_i^{pat}]$ can be found in Fig. 3, and the width $[W_i^{trans}]$ and length $[L_i^{trans}]$ of the impedance transformer can be found in Fig. 4. Thus, all parameters of the initial TSPAA can be obtained.

C. SIMULATION-BASED OPTIMIZATION

Although the resonant parameters are extracted from the uniform array environment where mutual coupling is considered, in an actual array, the element size and element spacing differ each other to cause different mutual coupling. Therefore, the error between the actual aperture distribution and the ideal aperture distribution is expected. In order to get the desired pattern, the initial array has to be optimized to reduce the error of the aperture distribution.

Actually, the mutual coupling between elements in a TSPAA is complicated and it is not easy to be calculated accurately [32]. For a linear traveling-wave array with uniform elements, the least square method was applied as optimized procedure to consider the mutual coupling [33]. However, we found that it could not work well for the TSPAAs in this work. The reason may be attributed to the large difference in element size and element spacing. In order to solve this problem, a simulation-based iteration procedure is proposed to optimize the initial array. In this procedure, the actual aperture distribution including amplitude and phase is extracted directly from the near-field probes which are set in the fringing edges of the patch elements in the HFSS simulation. The actual phase distribution $[\Phi_i]$ is derived from the phase of the probes, and the actual amplitude distribution $[A_i]$ can be expressed as

$$A_{\mathrm{i}} = a * \left|\overrightarrow{E_i^x}\right| * \Delta L * W_i^{pat} \tag{15}$$

where a is the coefficient independent of the elements, whose detailed description can be found in [34], $\overrightarrow{E_i^x}$ is the x component of the fringing electric field at the open end of the ith patch, and ΔL is the extended length of the patch due to the open-end effect, which depends on the height and the relative dielectric constant of the substrate.

In the kth iteration, the actual amplitude distribution $[A_i]$ and the actual phase distribution $[\Phi_i]$ are gotten from a full-wave simulation of an actual array. Then, the actual conductance distribution $[G_{i,\mathrm{probe}}^{pat}]$ and phase difference between adjacent elements $[P_{i,\mathrm{probe}}^{pat}]$ are deduced from (8) and (10), respectively. After that, a trial and error algorithm proposed in [33] is applied to reduce the error between the actual aperture distribution and the ideal aperture distribution, which can be written as

$$G_{i,k}^{pat} = G_{i,k-1}^{pat} * \left(1 + w_g * \left(G_{i,\mathrm{ideal}}^{pat} - G_{i,\mathrm{probe}}^{pat}\right)/G_{i,\mathrm{probe}}^{pat}\right) \tag{16}$$

$$P_{i,k} = P_{i,k-1} + w_p * \left(P_{i,\mathrm{probe}} - P_{i,\mathrm{ideal}}\right) \tag{17}$$

where $G_{i,\mathrm{ideal}}^{pat}$ and $P_{i,\mathrm{ideal}}$ are the ideal conductance and phase of the ith patch, respectively, $G_{i,k}^{pat}$ and $P_{i,k}$ are the amendatory conductance and phase of the ith patch in the kth iteration, respectively, $G_{i,k-1}^{pat}$ and $P_{i,k-1}$ are for the (k-1)th iteration, and w_g and w_p donate the inertia weight of the conductance and the phase difference in the iteration procedure, respectively, whose values are both set as 0.6 in this work. In the initial iteration, $G_{i,0}^{pat}$ and $P_{i,0}$ are equal to $G_{i,\mathrm{ideal}}^{pat}$ and $P_{i,\mathrm{ideal}}$, respectively. After every iteration, the structure parameters of the TSPAA will update by $G_{i,k}^{pat}$ and $P_{i,k}$ for the next iteration. The iteration algorithm terminates when the error reduces to a specified value. It is found that the iteration procedure can converge after several attempts in most cases. The reason may be attributed to the resonant parameters extracted from the uniform array which approximately takes the mutual coupling into account.

IV. DESIGN METHOD VERIFICATION

A. LOW-SIDELOBE ARRAY

To validate the proposed method, a 14-element TSPAA with low-sidelobe broadside radiation pattern is implemented. Different from the conventional traveling-wave arrays, the one using reflection-canceling elements can obtain broadside radiation pattern through tapered amplitude distribution [25]–[27]. The maximum element conductance greater than 1 is required to obtain tapered amplitude distribution for most cases. For a 14-element linear array with taylor-weighted amplitude distribution, the required variation range of radiating conductor is [0.026, 1.226] to obtain -23dB SLL. However, the variation range of radiating conductance for the proposed reflection-cancelling element is only [0.007, 0.553], which is not sufficient for the low-sidelobe array. Therefore, both amplitude and phase distribution are involved to design the low-sidelobe array through the proposed method in Section III.

The angle range of the mainlobe is set as [-5°, 5°], which means that the half-power beamwidth is about 10°. The angle range of the sidelobe is set as [-90°, -7°] and [7°, 90°], where the desired SLL is -20dB. Considering the design margin, the goal of SLL is set as -23dB. The GA procedure is used to synthesize the initial array. After some attempts, the number of the elements is set as 14. The amplitude distribution and phase distribution are shown in Fig. 7(a), and the comparison of the ideal and synthesized E-plane radiation patterns of the low-sidelobe array are shown in Fig. 7(b). The synthesized results of the radiation pattern reach the goal in spite of the increase of the SLL by 0.5dB. It is worth noting that the array except the last RML has a tapered amplitude distribution, and the last two elements have obvious different phase from

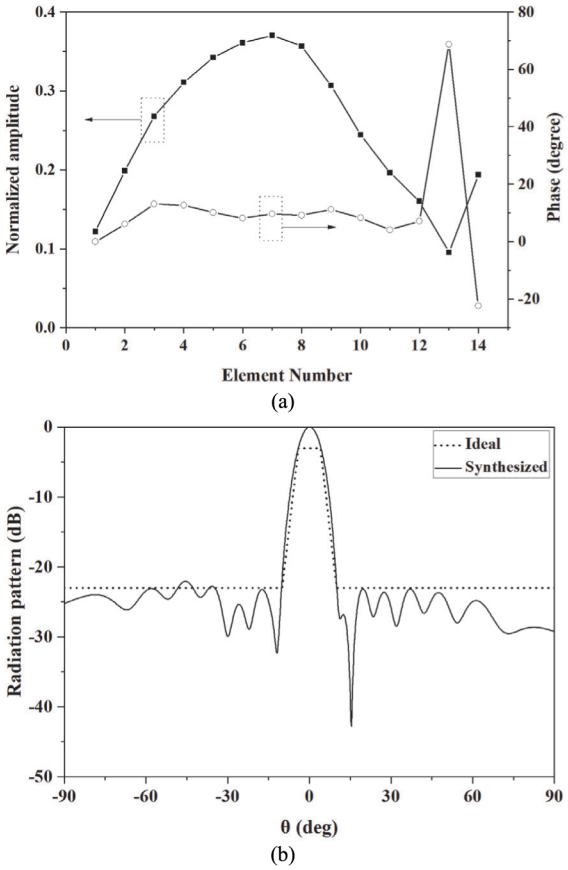

FIGURE 7. (a) Synthesized normalized amplitude and phase distribution of the low-sidelobe array, (b) comparison of the ideal and synthesized E-plane radiation patterns of the low-sidelobe array.

other elements. The full-wave simulated radiation pattern of the initial array is shown in Fig. 8. The simulated SLL is -21.2dB, which increases by 1.3dB compared with the synthesized result. Besides, the symmetry of the main lobe deteriorates. Then, the simulation-based iteration procedure is used to optimize the initial array. Comparison of the simulated radiation pattern between the initial array and optimized array is demonstrated in Fig. 8. It can be seen that the symmetry of the main lobe is improved, and the simulated SLL is lower than -21dB. A microstrip-to-GCPW-to-cable transition is applied to feed the proposed array. The geometry of the array is shown Fig. 9. The parameter values of the optimized array are given in Table. 1.

The low-sidelobe array is fabricated and measured. The prototype of the antenna is shown in Fig. 10. The simulated and measured reflection coefficients are shown in Fig.11. The measured resonant frequency shifts to 24.205GHz, which is slight greater than the simulated result by 0.08GHz. Both the simulated and measured reflection coefficient is lower than -12dB over the ISM 24GHz band. The simulated and measured radiation patterns at 24.125GHz are presented in Fig.12. The measured SLL is lower than -21.7dB, which is about 0.5dB better than the simulated result. The beam direction shifts about 0.5° from the broadside, which is corresponding to the shift of the resonant frequency.

TABLE 1. Geometric parameters of optimized low-sidelobe array elements. (UNIT: mm).

i	W_i^{pat}	L_i^{pat}	S_i^{pat}	W_i^{trans}	L_i^{trans}
1	0.943	3.446	——	0.223	1.943
2	1.410	3.334	7.121	0.231	1.941
3	1.892	3.246	6.941	0.246	1.938
4	2.283	3.193	6.973	0.260	1.933
5	2.682	3.150	6.914	0.280	1.929
6	3.128	3.114	6.789	0.308	1.921
7	3.660	3.080	6.577	0.335	1.917
8	4.223	3.053	6.452	0.377	1.910
9	4.465	3.043	6.253	0.396	1.906
10	4.438	3.045	6.336	0.392	1.908
11	4.500	3.042	6.366	0.391	1.908
12	4.500	3.042	6.172	0.395	1.906
13	3.100	3.115	5.291	0.306	1.921
14	4.500	2.947	7.569	0.533	1.887

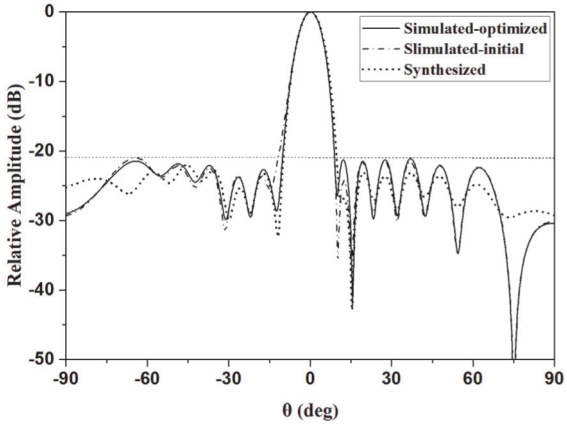

FIGURE 8. Simulated E-plane radiation pattern of the initial low-sidelobe array and the optimized low-sidelobe array.

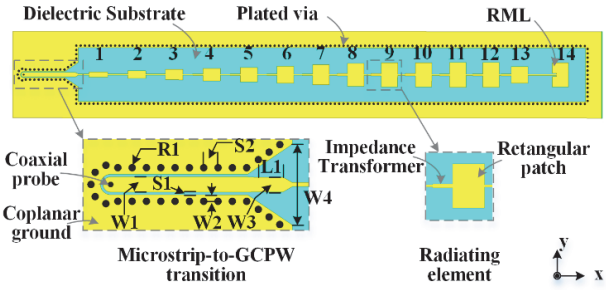

FIGURE 9. Configuration of the proposed low-sidelobe array ($W1 = 0.850$mm, $W2 = 0.360$mm, $W3 = 0.800$mm, $W4 = 4.500$mm, $R1 = 0.200$mm, $L1 = 1.500$mm, $S1 = 0.150$mm, $S2 = 0.800$mm).

Similar phenomenon can be found in [25], which is attributed to the PCB fabrication error of the right angle. The measured antenna gain is also shown in Fig. 11. It can be seen that the measured gain is larger than 15.95dBi, which is about 0.39dB lower than the simulated result. Considering the insertion loss of the 2.92mm connector and the fabrication error, the measured results show reasonable agreement with the simulated results. Thus, it is concluded that the TSPAA with low-sidelobe and broadside beam can be realized by the proposed design method.

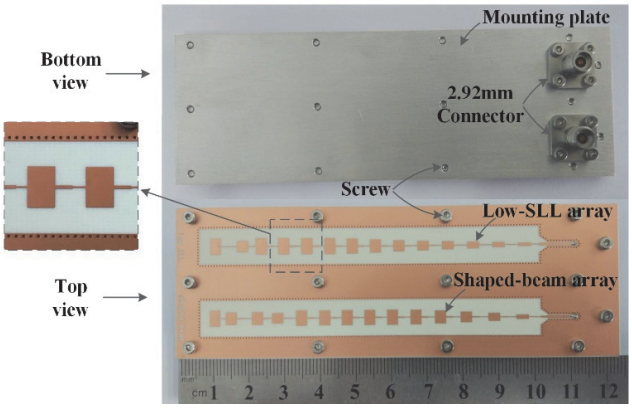

FIGURE 10. Photograph of the fabricated array antennas.

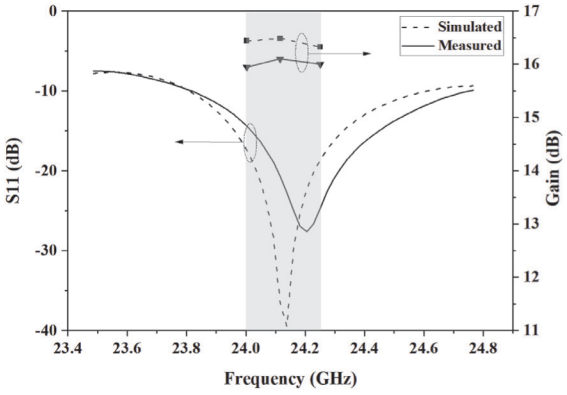

FIGURE 11. Comparison of the reflection coefficient (S11) and antenna gain between simulated results and measured results of the low-sidelobe array.

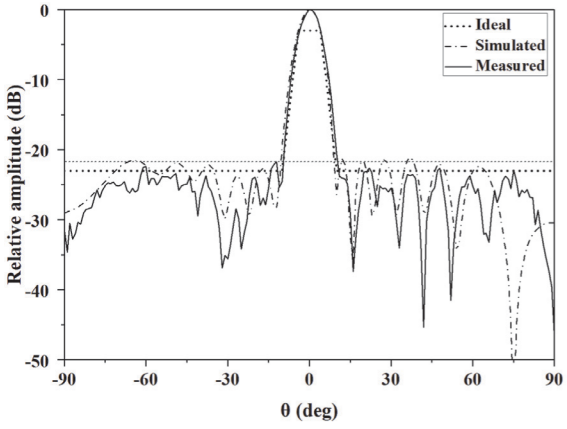

FIGURE 12. Comparison of the radiation patterns of the low-sidelobe array among the ideal, simulated and measured results.

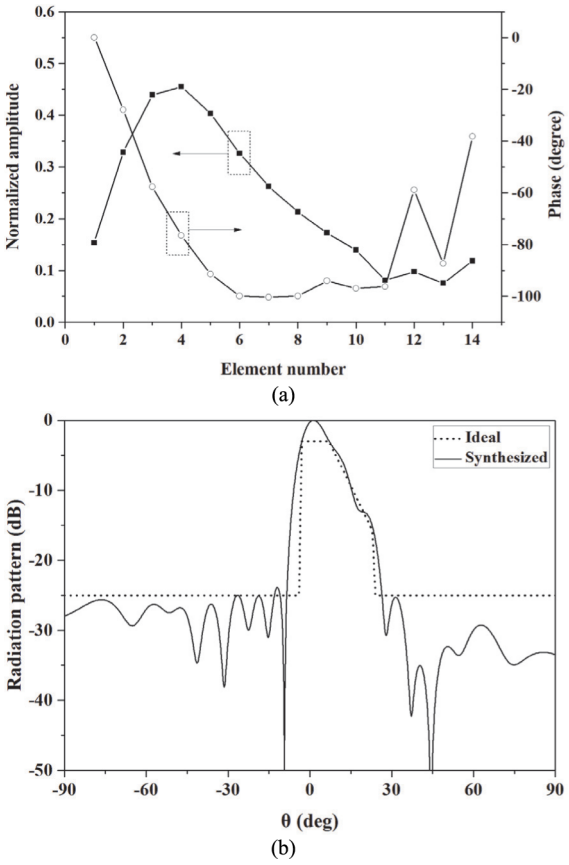

FIGURE 13. (a) Synthesized normalized amplitude and phase distribution of the low-sidelobe array, (b) comparison of the ideal and synthesized E-plane radiation patterns of the shaped-beam array.

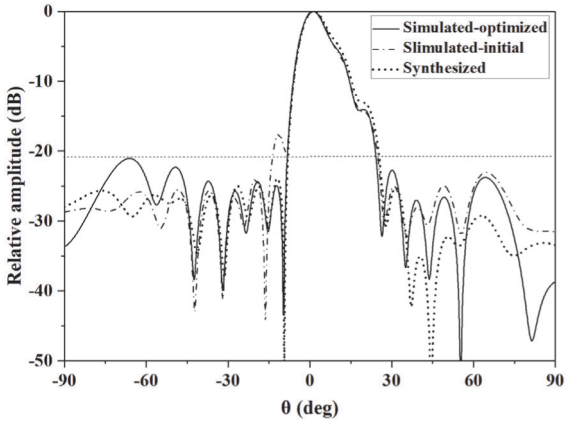

FIGURE 14. Comparison of the simulated radiation pattern of the initial shaped-beam array and the synthesized optimum radiation pattern of the shaped-beam array.

B. SHAPED-BEAM ARRAY

In order to verify that the proposed method is effective for a flexible beam, a 14-element TSPAA with shaped-beam radiation pattern is implemented. The angle range of the mainlobe is set as [-3°, 23°], where the drop region is [7°, 23°]. The angle range of the sidelobe is set as [-90°, -10°] and [28°,90°], of which the desired SLL is -20dB. Considering the design margin, the goal of the SLL is set as -25dB. The synthesized amplitude and phase distributions of the initial array are shown in Fig. 13(a). The ideal distributions are shown in Fig. 13(b). It can be seen that the synthesized radiation pattern reaches the goal in spite of that the SLL increased by 1.1dB. The comparison of the simulated radiation pattern of the initial array and the synthesized optimum radiation pattern is shown in Fig. 14. The simulated result of the mainlobe agrees well with the synthesized result, where the difference is less than 1.4dB. However, the first sidelobe

TABLE 2. Geometric parameters of optimized shaped-beam array elements. (UNIT: mm).

i	W_i^{pat}	L_i^{pat}	S_i^{pat}	W_i^{trans}	L_i^{trans}
1	1.225	3.400	-----	0.224	1.944
2	2.224	3.193	7.689	0.260	1.933
3	2.964	3.099	7.654	0.312	1.924
4	3.664	3.060	7.148	0.364	1.911
5	4.140	3.046	6.840	0.390	1.908
6	4.279	3.046	6.563	0.391	1.908
7	4.269	3.047	6.344	0.390	1.909
8	4.284	3.046	6.323	0.391	1.908
9	4.154	3.045	6.200	0.393	1.908
10	4.273	3.044	6.404	0.392	1.907
11	2.945	3.123	6.578	0.298	1.924
12	3.556	3.053	5.545	0.378	1.910
13	3.447	3.067	7.306	0.358	1.911
14	4.500	2.947	4.582	0.533	1.887

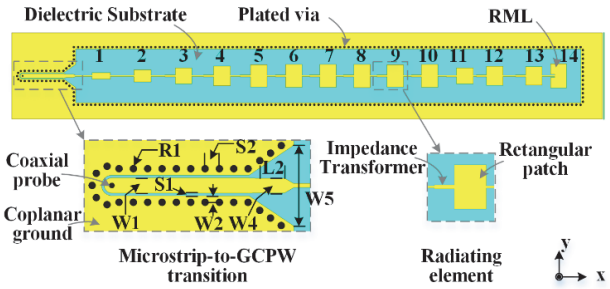

FIGURE 15. Configuration of the proposed shaped-beam array ($W1 = 0.850$mm, $W2 = 0.360$mm, $W4 = 0.600$mm, $W5 = 0.600$mm, $R1 = 0.200$mm, $L1 = 1.250$mm, $S1 = 0.150$mm, $S2 = 0.800$mm).

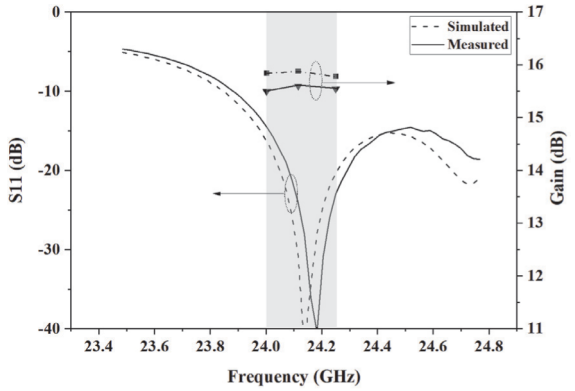

FIGURE 16. Comparison of the reflection coefficient (S11) and antenna gain between simulated results and measured results of the shaped-beam array.

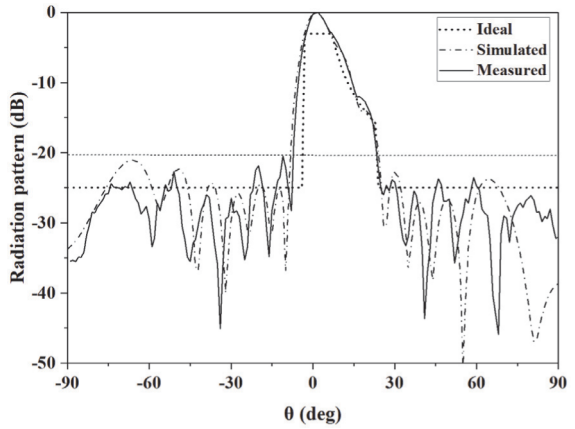

FIGURE 17. Comparison of the radiation patterns of the shaped-beam array among the ideal, simulated and measured results.

deteriorates by 6.3dB, which is -17.6dB compared with the synthesized result of -23.9dB.

The simulation-based iteration procedure is used to optimize the initial array. Comparison of the simulated radiation pattern between the initial array and optimized array is shown in Fig. 14. It can be seen that the first sidelobe is suppressed from -17.6dB to -25dB, and the sidelobe level in the whole sidelobe region is lower than -21dB. In addition, the main-lobe remains approximately the same. Similar with the low-sidelobe array, a microstrip-to-GCPW-to-cable transition is applied to feed the shaped-beam array, as shown in Fig. 15. The geometry parameter values of the optimized array are given in Table II.

The prototype of the shaped-beam array is also shown in Fig. 10. The simulated and measured reflection coefficients are presented in Fig.16. Compared with the simulated result, the measured resonant frequency shifts to a higher frequency by 0.04GHz, from 24.125GHz to 24.185GHz. Both the simulated and measured reflection coefficients are lower than -14dB over the ISM 24GHz band.

The simulated and measured radiation patterns at 24.125GHz are presented in Fig. 17. A slight difference less than -1.9dB can be found around 18° on the main beam. The measured SLL is less than -20.4dB, which is 0.6dB higher than the simulated result. It is worth to note that the sidelobe at around -65° is increased by about 3dB, but the first sidelobe is decreased by 4.6dB. The measured antenna gain shown in Fig. 16 is greater than 15.5dBi, which is about 0.28dB lower than the simulated result. The measured results show reasonable agreement with the simulated results considering the insert loss and the fabrication error, which demonstrates that the TSPAA with shaped-beam radiation pattern can be realized by the proposed design method.

V. CONCLUSION

This paper proposed a new method to design and synthesize the TSPAAs with flexible radiation patterns. The operating frequency is set at ISM 24GHz. The method is based on a novel reflection-canceling element, where a quarter-wave impedance transformer is introduced to suppress the reflection of the patch element. To obtain an arbitrary beam, the GA procedure is conducted to produce the initial array, and a simulation-based iteration procedure is proposed to optimize the initial array with taking into account the actual mutual coupling. To evaluate the proposed method, two different types of linear arrays, a low-sidelobe TSPAA and a shaped-beam TSPAA, are designed, simulated, fabricated and measured, respectively. The measured results show that the low-sidelobe TSPAA achieves broadside radiation pattern

with SLL lower than -21.7dB, while the shaped-beam TSPAA achieves desired main beam with SLL lower than -20.4dB. The proposed method provides satisfactory robustness for a flexible beam. It is very promising to develop planar antennas for millimeter-wave radar sensors operating at 24GHz, 60GHz, 77GHz, and other frequency bands.

ACKNOWLEDGMENTS

The authors would like to thank Hunan Nanoradar Science & Technology Co., Ltd., for development of millimeter-wave radars based on the antennas designed with the proposed method, and providing the detailed test results of these radars.

REFERENCES

[1] A. G. Derneryd, "Linearly polarized microstrip antennas," *IEEE Trans. Antennas Propag.*, vol. 24, no. 6, pp. 846–851, Nov. 1976.

[2] D. M. Pozar, "Microstrip antennas," *Proc. IEEE*, vol. 80, no. 1, pp. 79–91, Jan. 1992.

[3] W. Lee, J. Kim, and Y. J. Yoon, "Compact two-layer rotman lens-fed microstrip antenna array at 24 GHz," *IEEE Trans. Antennas Propag.*, vol. AP-59, no. 2, pp. 460–466, Feb. 2011.

[4] H. Wang, Z. Zhang, Y. Li, and M. Iskander, "A switched beam antenna with shaped radiation pattern and interleaving array architecture," *IEEE Trans. Antennas Propag.*, vol. 63, no. 7, pp. 2914–2921, Jul. 2015.

[5] W. Yang, K. Ma, K. S. Yeo, and W. M. Lim, "A compact high-performance patch antenna array for 60-GHz applications," *IEEE Antennas Wireless Propag. Lett.*, vol. 15, pp. 313–316, 2016.

[6] C. G. Salzburg, T. Vaupel, T. Bertuch, M. Wilhelm, T. Wichmann, and S. T. Alfageme, "Feasibility of an automotive radar antenna at 77 GHz on LTCC substrate," *IET Radar, Sonar Navigat.*, vol. 12, no. 10, pp. 1172–1178, 2018.

[7] R. J. Mailloux, J. F. McIlvenna, and N. Kernweis, "Microstrip array technology," *IEEE Trans. Antennas Propag.*, vol. AP-29, no. 1, pp. 25–37, Jan. 1981.

[8] T. Metzler, "Microstrip series arrays," *IEEE Trans. Antennas Propag.*, vol. 29, no. 1, pp. 174–178, Jan. 1981.

[9] T. Yuan, N. Yuan, and L.-W. Li, "A novel series-fed taper antenna array design," *IEEE Antennas Wireless Propag. Lett.*, vol. 7, pp. 362–365, 2008.

[10] Z. Chen and S. Otto, "A taper optimization for pattern synthesis of microstrip series-fed patch array antennas," in *Proc. Eur. Wireless Technol. Conf.*, Rome, Italy, Sep. 2009, pp. 160–163.

[11] J. Xu, W. Hong, H. Zhang, G. Wang, Y. Yu, and Z. H. Jiang, "An array antenna for both long- and medium-range 77 GHz automotive radar applications," *IEEE Trans. Antennas Propag.*, vol. 65, no. 12, pp. 7207–7216, Dec. 2017.

[12] P. A. Dzagbletey and Y. B. Jung, "Stacked microstrip linear array for millimeter-wave 5G baseband communication," *IEEE Antennas Wireless Propag. Lett.*, vol. 17, no. 5, pp. 780–783, May 2018.

[13] P. Hallbjorner, M. Bergstrom, M. Boman, P. Lindberg, E. Ojefors, and A. Rydberg, "Millimetre-wave switched beam antenna using multiple travelling-wave patch arrays," *IEE Proc. Microw., Antennas Propag.*, vol. 152, no. 6, pp. 551–555, Dec. 2005.

[14] S. Cheng, E. Öjefors, P. Hallbjörner, and A. Rydberg, "Compact reflective microstrip phase shifter for traveling wave antenna applications," *IEEE Microw. Wireless Compon. Lett.*, vol. 16, no. 12, pp. 431–433, Jul. 2006.

[15] E. Ojefors, S. Cheng, K. From, I. Skarin, P. Hallbjorner, and A. Rydberg, "Electrically steerable single-layer microstrip traveling wave antenna with varactor diode based phase shifters," *IEEE Trans. Antennas Propag.*, vol. 55, no. 9, pp. 2451–2460, Sep. 2007.

[16] S. Karimkashi, G. Zhang, A. A. Kishk, W. Bocangel, R. Kelley, J. Meier, and R. D. Palmer, "Dual-polarization frequency scanning microstrip array antenna with low cross-polarization for weather measurements," *IEEE Trans. Antennas Propag.*, vol. 61, no. 11, pp. 5444–5452, Nov. 2013.

[17] B. Jones, F. Chow, and A. Seeto, "The synthesis of shaped patterns with series-fed microstrip patch arrays," *IEEE Trans. Antennas Propag.*, vol. AP-30, no. 6, pp. 1206–1212, Nov. 1982.

[18] D. G. Babas and J. N. Sahalos, "Synthesis method of series-fed microstrip antenna arrays," *Electron. Lett.*, vol. 43, no. 2, pp. 78–80, Jan. 2007.

[19] J. Jayasinghe, J. Anguera, and D. Uduwawala, "Genetic algorithm optimization of a high-directivity microstrip patch antenna having a rectangular profile," *Radioengineering*, vol. 22, no. 3, pp. 700–707, 2013.

[20] K. Sakakibara, J. Hirokawa, M. Ando, and N. Goto, "A slotted waveguide array using reflection-cancelling slot pairs," in *Proc. IEEE Antennas Propag. Soc. Int. Symp.*, Ann Arbor, MI, USA, Jun./Jul. 1993, pp. 1570–1573.

[21] S. Park, J. Hirokawa, and M. Ando, "Analysis and design of a waveguide slot and a reflection-canceling inductive wall," in *Proc. IEEE Top. Conf. Wireless Commun. Technol.*, Oct. 2003, pp. 362–363.

[22] S. Park, Y. Tsunemitsu, J. Hirokawa, and M. Ando, "Center feed single layer slotted waveguide array," *IEEE Trans. Antennas Propag.*, vol. 54, no. 5, pp. 1474–1480, May 2006.

[23] S. Park, Y. Okajima, J. Hirokawa, and M. Ando, "A slotted post-wall waveguide array with inter-digital structure for 45-deg linear and dual polarization," in *Proc. IEEE Antennas Propag. Soc. Symp.*, Monterey, CA, USA, Jun. 2004, pp. 2368–2371.

[24] F. D. L. Peters, S. O. Tatu, and T. A. Denidni, "Design of traveling-wave equidistant slot antennas for millimeter-wave applications," in *Proc. IEEE Int. Symp. Antennas Propag.*, Jul. 2011, pp. 3037–3040.

[25] Y. Hayashi, K. Sakakibara, M. Nanjo, S. Sugawa, N. Kikuma, and H. Hirayama, "Millimeter-wave microstrip comb-line antenna using reflection-canceling slit structure," *IEEE Trans. Antennas Propag.*, vol. 59, no. 2, pp. 398–406, Feb. 2011.

[26] S. Sugawa, K. Sakakibara, N. Kikuma, and H. Hirayama, "Low-sidelobe design of microstrip comb-line antennas using stub-integrated radiating elements in the millimeter-wave band," *IEEE Trans. Antennas Propag.*, vol. 60, no. 10, pp. 4699–4709, Oct. 2012.

[27] S. Afoakwa and Y.-B. Jung, "Wideband microstrip comb-line linear array antenna using stubbed-element technique for high sidelobe suppression," *IEEE Trans. Antennas Propag.*, vol. 65, no. 10, pp. 5190–5199, Oct. 2017.

[28] J. M. Johnson and V. Rahmat-Samii, "Genetic algorithms in engineering electromagnetics," *IEEE Antennas Propag. Mag.*, vol. 39, no. 4, pp. 7–21, Aug. 1997.

[29] K.-K. Yan and Y. Lu, "Sidelobe reduction in array-pattern synthesis using genetic algorithm," *IEEE Trans. Antennas Propag.*, vol. 45, no. 7, pp. 1117–1122, Jul. 1997.

[30] D. S. Weile and E. Michielssen, "Genetic algorithm optimization applied to electromagnetics: A review," *IEEE Trans. Antennas Propag.*, vol. 45, no. 3, pp. 343–353, Mar. 1997.

[31] J. Yin, Q. Wu, C. Yu, H. Wang, and W. Hong, "Low-sidelobe-level series-fed microstrip antenna array of unequal interelement spacing," *IEEE Antennas Wireless Propag. Lett.*, vol. 16, pp. 1695–1698, 2017.

[32] S. Sengupta, D. R. Jackson, and S. A. Long, "A method for analyzing a linear series-fed rectangular microstrip antenna array," *IEEE Trans. Antennas Propag.*, vol. 63, no. 8, pp. 3731–3736, Aug. 2015.

[33] L. Qiu, K. Xiao, S. L. Chai, H. Y. Qi, and J. J. Mao, "A double-layer shaped-beam traveling-wave slot array based on SIW," *IEEE Trans. Antennas Propag.*, vol. 64, no. 11, pp. 4639–4647, Nov. 2016.

[34] R. Garg, P. Bhartia, I. Bahl, and A. Ittipiboon, *Microstrip Antenna Design Handbook*. Boston, MA, USA: Artech House, 2001.

HAO YI was born in Yueyang, China, in 1988. He received the B.E. and master's degrees in electromagnetic fields and microwave technology from Xidian University, Xi'an, China, in 2011 and 2014, respectively, where he is currently pursuing the Ph.D. degree in electromagnetic fields and microwave technology.

He joined a startup company focusing on millimeter wave radars as a Senior Antenna Engineer, in 2014. He has authored over ten Chinese patents. His research interests include millimeter wave antenna array, automotive radar antenna, reflectarray, and metasurface antenna.

LONG LI (M'06–SM'11) was born in Guizhou, China. He received the B.E. and Ph.D. degrees in electromagnetic fields and microwave technology from Xidian University, Xi'an, China, in 1998 and 2005, respectively.

He joined the School of Electronic Engineering, Xidian University, in 2005, and became a Full Professor, in 2010. He was a Senior Research Associate with the Wireless Communications Research Center, City University of Hong Kong, in 2006. He received the Japan Society for Promotion of Science (JSPS) Postdoctoral Fellowship and visited Tohoku University, Sendai, Japan, as a JSPS Fellow, from November 2006 to November 2008. He was a Senior Visiting Scholar with the Pennsylvania State University, USA, from December 2013 to July 2014. He is currently a Full Professor with the School of Electronic Engineering, Xidian University. He is also the Director of the Key Laboratory of High Speed Circuit Design and EMC, Ministry of Education, China. He has authored or coauthored over 100 papers in refereed journal. His research interests include metamaterials, computational electromagnetics, electromagnetic compatibility, novel antennas, and wireless power transfer and harvesting technology.

Prof. Li received the Nomination Award of National Excellent Doctoral Dissertation of China, in 2007. He was a recipient of the Best Paper Award in the International Symposium on Antennas and Propagation, in 2008. He received the Program for New Century Excellent Talents in University of the Ministry of Education of China, in 2010. He received the First Prize of awards for Scientific Research Results offered by the Shaanxi Provincial Department of Education, China, in 2013. He received the IEEE APS Raj Mittra Travel Grant Senior Researcher Award, in 2014. He received the Shaanxi Youth Science and Technology Award, in 2016. He is a Senior Member of the Chinese Institute of Electronics (CIE).

JIAQI HAN was born in Jiazuo, China, in 1991. He is currently pursuing the Ph.D. degree in electromagnetic fields and microwave technology with Xidian University, Xi'an, China. His research interests include metasurface design, reconfigurable metasurface applications, and metasurface radiation analysis.

YAN SHI (M'07–SM'16) received the B.Eng. and Ph.D. degrees in electromagnetic fields and microwave technology from Xidian University, Xi'an, China, in 2001 and 2005, respectively.

He joined the School of Electronic Engineering, Xidian University, in 2005, and became a Full Professor, in 2011. From 2007 to 2008, he was a Senior Research Associate with the City University of Hong Kong, Hong Kong. From 2009 to 2010, he was a Visiting Postdoctoral Research Associate with the University of Illinois at Urbana—Champaign, Champaign, IL, USA. He has authored or coauthored over 100 papers in refereed journal and one book entitled notes on *Catastrophe Theory* (SciPress, 2015). His current research interests include computational electromagnetics, metamaterial, antenna, and electromagnetic compatibility. He is a Senior Member of the Chinese Institute of Electronics. He received the Program for New Century Excellent Talents in university awarded by the Ministry of Education of China, in 2011, the New Scientific and Technological Star of Shaanxi Province awarded by the Education Department of Shaanxi Provincial Government, in 2013, the First Prize for the Scientific Research Results of High Education of Shaanxi Province awarded by the Education Department of the Shaanxi Provincial Government, in 2013, and the Second Prize of awards of Science and Technology awarded by the Shaanxi Province Government, in 2015.